RSC Advances

PAPER

View Article Online
View Journal | View Issue

Cite this: *RSC Adv.*, 2022, **12**, 15038

Facile one-pot method of AuNPs/PEDOT/CNT composites for simultaneous detection of dopamine with a high concentration of ascorbic acid and uric acid

Shaohua Chen, * Wenliang Chen, Yihua Wang, Xiufang Wang, Yi Ding, Donglin Zhao and Jiyu Liu

In this research, a facile one-pot method was used to synthesize gold/poly-3,4-ethylene-dioxythiophene/carbon nanotube (AuNPs/PEDOT/CNTs) composite material. The composite material was investigated by Fourier Transform Infrared spectroscopy (FTIR), X-ray diffraction (XRD) and Scanning Electron Microscopy (SEM). Then the synthesized nanocomposite material was dropped on a bare glassy carbon electrode (GCE) to improve the detection performance of dopamine with a high concentration of ascorbic acid and uric acid. The electrochemical behavior of AuNPs/PEDOT/CNTs/GCE was studied by Cyclic Voltammetry (CV), Differential Pulse Voltammetry (DPV) and electrochemical impedance spectroscopy (EIS). Under optimum conditions, AuNPs/PEDOT/CNTs/GCE showed a good linear response in the concentration range from 9.14 to 29.704 μM with a detection limit (LOD) and sensitivity of 0.283 μM and 1.557 μA μM^{-1}, respectively. This sensor was applied to detect practical samples with good average recovery. It also exhibited good reproducibility and stability.

Received 25th February 2022
Accepted 29th April 2022

DOI: 10.1039/d2ra01262f

rsc.li/rsc-advances

1 Introduction

Dopamine (DA) is an important neurotransmitter that regulates human emotions and cognition. The average content of DA in human serum is about 10^{-6} to 10^{-9} M. Too much or too little can cause serious neurological diseases, such as Parkinson's disease and schizophrenia.[1–3] Therefore, cost-effective detection methods are necessary. Traditional methods for detecting dopamine include, but are not limited to, spectrophotometry,[4,5] fluorescence spectroscopy,[6,7] high performance liquid chromatography, and electrochemical analysis.[8–12] Spectrophotometry utilizes the unique enol structure of dopamine, which when combined with certain compounds can generate colored compounds that selectively absorb light. The method is simple and quick to operate, but the accuracy is not high and the sensitivity is not good. Its detection limit is usually on the order of 10^{-5}, which is much higher than the dopamine content in the human body. Fluorescence spectroscopy utilizes that dopamine has a conjugated π bond structure and the molecule is a rigid plane, which can fluoresce under ultraviolet irradiation. This method is sensitive and can detect dopamine at low concentrations, but its application range is narrow and it is poor for qualitative analysis. High-performance liquid chromatography has high resolution and can detect low-concentration dopamine content, but the operation is complicated and the detection time is long. Among these detection and analysis methods, electrochemical analysis methods can usually meet the conditions of cost-effectiveness and efficiency, but interfering substances such as ascorbic acid (AA) and uric acid (UA) contained in human serum have an oxidation potential similar to that of DA on the bare electrode.[13] And the concentration of interfering substances is much higher than DA. In addition, fouling of bare electrodes also degrades the sensor response, due to the fact that compounds undergo many secondary reactions after earlier electron transfer, producing insulating species that deactivate the electrode surface.[14] Therefore, researchers are devoted to solving these problems by developing various modified electrodes. Chemical modification of the electrode surface can effectively reduce the oxidation potential of the reaction, improve the transfer rate of electrons between the electrode, the reactive site and the detection substance, and at the same time improve the selective response to the detection substance.

Carbon nanotubes (CNTs) have high specific surface area and electrical conductivity, and the surface of carbon nanotubes after acid treatment usually contains various oxygen-containing functional groups. It has been reported that the oxygen content on the surface of carbon nanotubes greatly affects the adsorption capacity of pollutants.[15] Compared with untreated carbon nanotubes, acidified carbon nanotubes are highly dispersed in solution and selectively adsorb positively charged dopamine due to their negative energy.

Anhui Key Laboratory of Advanced Building Materials, Anhui Jianzhu University, Hefei 230022, Anhui Province, P. R. China. E-mail: chshaohua@126.com

Gold,[16,17] silver, platinum[18,19] and other noble metal nanoparticles have attracted much attention from researchers due to their excellent electrical conductivity and electrocatalytic properties. Gold nanoparticles (AuNPs) have promising applications in electrochemical detection. Its special structure, low toxicity and biocompatibility make it suitable for sensing applications.[20,21] However, in practical applications, gold nanoparticles tend to agglomerate, which affects the surface area and catalysis. Combining with carbon nanotubes can effectively solve this problem, and carbon nanotubes can provide abundant active sites for gold nanoparticles due to the existence of defects, and improve the dispersibility and electroactive surface properties of composites.

Poly-3,4-ethylenedioxythiophene (PEDOT) is an excellent conducting polymer that has been widely used in electrochemistry for its excellent mechanical, electronic and chemical properties.[22] For example, its biocompatibility and environmental stability are superior to other conductive polymers, and the sulfur element it contains can form stable chemical bonds with gold nanoparticles to improve the conductivity of the composite.

In recent years, researchers have focused on binary composites of carbon nanomaterials,[23–25] noble metals,[26–28] transition metal oxide nanoparticles,[29–31] and biomolecules.[32–34] There are few studies on ternary composites based on carbon nanomaterials. As far as we know, the research on electrochemical detection of DA mainly focuses on the research of carbon nanomaterials-metal or polymer-metal binary composites, and the preparation and modification process is relatively complicated and tedious. In this study, the ternary nanocomposites of gold nanoparticles/poly-3,4-ethylenedioxythiophene/modified carbon nanotubes (AuNPs/PEDOT/CNTs), without the addition of other oxidants and stabilizers, through easy one-pot preparation, an electrochemical sensor capable of efficiently detecting DA in the presence of high concentrations of AA and UA was designed for the first time.

2 Experimental

2.1 Chemical and reagents

3,4-Ethylenedioxythiophene (EDOT), hydrated chloroauric acid ($HAuCL_4 \cdot 4H_2O$), absolute ethanol, potassium chloride (KCl), dipotassium hydrogen phosphate (K_2HPO_4), potassium dihydrogen phosphate (KH_2PO_4), lemon sodium ($C_6H_5Na_3O_7 \cdot 2H_2O$) and carbon nanotubes were purchased from McLean, dopamine hydrochloride (20 mg : 2 mL) was purchased from Shanghai Harvest Pharmaceutical. Co., Ltd., 98% concentrated sulfuric acid and concentrated nitric acid were purchased from Xilong Chemical Co., Ltd., potassium ferricyanide ($K_3[Fe(CN)_6]$) was purchased from Shanghai Shanpu Chemical Co., Ltd. Except for carbon nanotubes, other reagents were of analytical grade and were used directly without further processing.

2.2 Instrumentation

The physical characterization of the synthesized products was obtained by Fourier transform infrared spectroscopy (FTIR) of Nicoley iS10, X-ray diffraction (XRD) and scanning electron microscope (SEM) of regulus8100. Shanghai Qingkai electrochemical workstation is used for cyclic voltammetry (CV), differential pulse voltammetry (DPV) and electrochemical impedance (EIS) measurements of three-electrode systems. A bare glassy carbon electrode (3 mm in diameter) was used as the working electrode, a platinum sheet electrode with a diameter of 1 mm was used as the auxiliary electrode saturated and the calomel electrode was used as the reference electrode.

2.3 Gold/poly3,4-ethylene-dioxythiophene/carbon nanotube (AuNPs/PEDOT/CNTs) nanocomposite material was synthesized *via* the facile one-pot method

Acid-treated CNTs were prepared according to the work of Luo[35] *et al.* 200 mg of CNTs was dispersed in 100 mL of 3 : 1 concentrated H_2SO_4 and HNO_3 solution, sonicated for 2 h, and the suspension kept at room temperature for 24 h. After the acid treatment, the carbon nanotubes were washed with deionized water until the washing solution was neutral. Finally, the carbon nanotubes were dried at 60 °C.

AuNPs/PEDOT/CNTs composites material was synthesized by CNTs, EDOT and reduction of Au(III) with the addition of $C_6H_5Na_3O_7$. Taking 500 μL of 2% chloroauric acid solution and CNTs into 100 mL of deionized water, heating and stirring until it boils. Then 10 μL EDOT mixed with 5 mL ethanol and 160 mg $C_6H_5Na_3O_7$ was added and kept stirring for 3 h. Finally, the suspension was washed with ethanol and deionized water by centrifugation, and dried at 60 °C for 18 h.

2.4 Preparation of modified electrodes by drop coating

CNTs and AuNPs/PEDOT/CNT composites material were prepared at a concentration of 1 mg mL^{-1}. The synthesized composites material were dispersed in deionized water and sonicated for 30 min. On the other hand, the bare glassy carbon electrode (GCE) was polished with alumina and then ultrasonically cleaned with deionized water, 1 : 1 ethanol aqueous solution, and deionized water for 1 min, respectively. After passing the test in potassium ferricyanide solution, rinsed and washed thoroughly. 8 μL of suspension solution was dropped on the surface of bare GCE, and dried at room temperature for 2 h.

2.5 Electrochemical measurement

All electrochemical experiments were carried out by using an electrochemical workstation (Shanghai Qingkai Experimental Equipment Co., Ltd.). A three-electrode system was used for each electrochemical analysis. The modified GCE was used as the working electrode, and the saturated calomel electrode and the platinum electrode were used as the reference electrode and auxiliary electrode, respectively. The CV and EIS curves of the electrodes were studied in a mixed solution of 5 mM potassium ferricyanide and 0.1 M KCl. The frequency range of EIS was 0.1 Hz to 1 MHz and the amplitude was 5 mV. The DPV curves of the electrodes were investigated in 0.1 M PBS solution with an amplitude of 100 mV.

3 Results and discussion

3.1 AuNPs/PEDOT/CNTs formation mechanism of composite materials

Hydroxylated or carboxylated carbon nanotubes are negatively charged in solution. EDOT monomer and Au ions are adsorbed on carbon nanotubes. Due to the existence of defects, Au will use defects as nucleation sites, and form nanoparticles in the presence of reducing agents. The acidified CNTs acted as dopants to balance the positive charges in the PEDOT backbone and intercalated as part of the formed polymer.

Fig. 1(a) showed that gold nanoparticles embedded and grew at the end of CNTs. The size of gold nanoparticles was about 25–50 nm. Fig. 1(c) and (d) showed the composite situation of the three materials. PEDOT film was also formed at the end of CNTs. It can be attributed to bonding effect of Au–S. The CNTs were pure and couldn't see any impurities. The diameter of CNTs was about 25–35 nm, and they wound randomly among each other to form 3D network structure.

FTIR is one of the most widely used tools for determining functional groups of compounds. It can be seen from Fig. 2 that the peaks at 1570 cm^{-1} and 1390 cm^{-1} can be attributed to the stretching vibration of C=C and C_β–C_β in the thiophene ring;[15] the peaks at 1250 cm^{-1} and 1070 cm^{-1} can be attributed to C–O–C stretching vibration in ethylenedioxy; the peaks at

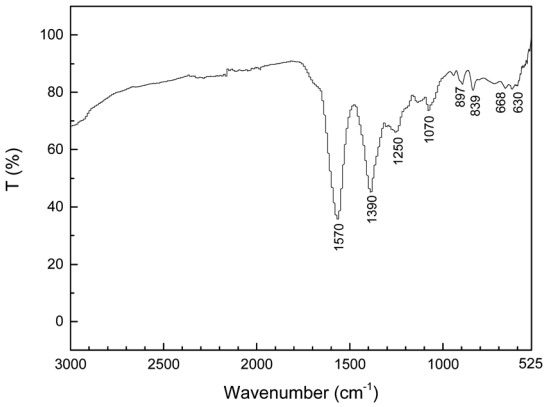

Fig. 2 FTIR spectra of composite material.

630 cm^{-1} and 897 cm^{-1} can be attributed to C–H in-plane bending vibration the peaks at 839 cm^{-1} and 668 cm^{-1} can be attributed to C–S stretching vibration in thiophene ring.[36]

The XRD pattern of PEDOT showed a broad characteristic peak at approximately $2\theta = 25.9°$, which is associated with intermolecular π–π stacking and can be attributed to the (020) reflective polymer backbone.[37] Furthermore, the characteristic peaks at $2\theta = 38.20°$, 44.36°, 64.75° and 77.60° correspond to the (111), (200), (220) and (311) planes of Au, respectively (Fig. 3).

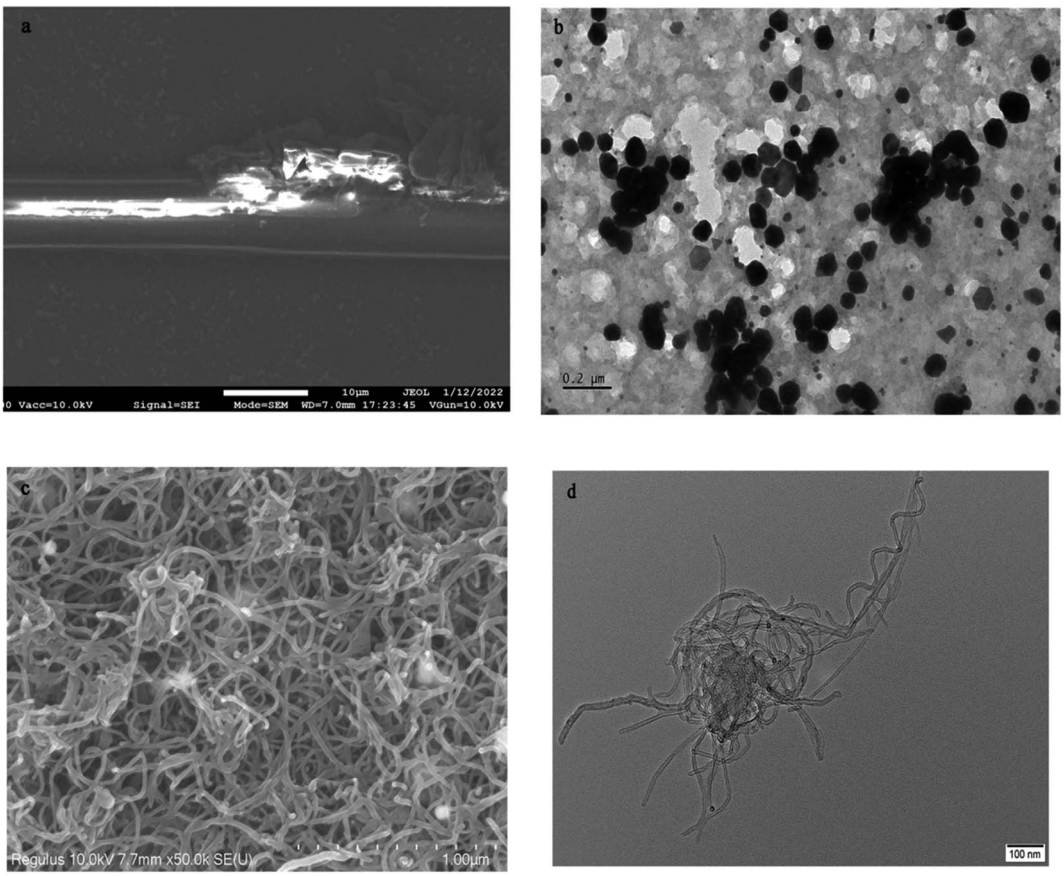

Fig. 1 SEM and TEM of composite material.

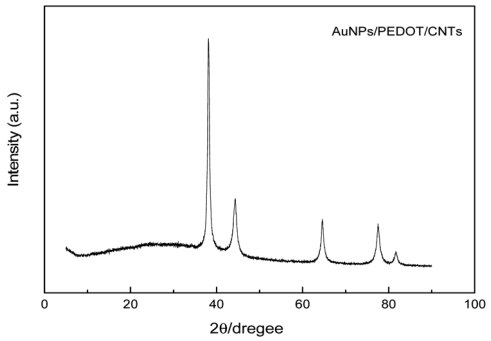

Fig. 3 XRD spectra of composite materials.

3.2 Electrochemical characterization of modified electrodes

The redox behaviors of bare GCE, CNTs/GCE and AuNPs/PEDOT/CNTs were investigated by cyclic voltammetry (CV). The electrochemical behaviors of the three electrodes at different scan rates were studied in the potential range of −0.2–0.6 V. Compared with other modified electrodes studied, AuNPs/PEDOT/CNTs showed more pronounced redox peaks (Fig. 4(a)). This means that AuNPs/PEDOT/CNTs have the best catalytic ability. It can be seen from Fig. 4(c) that the redox current and peak interval of AuNPs/PEDOT/CNTs/GCE increase with the increase of scan rate. The peak current is proportional to the square root of the scan rate(Fig. 4(d)). According to theory, eqn (1) and (2), if the peak interval ΔE is 59 mV, the ratio of peak currents is approximately 1, both parameters indicating that the process is an ideal reversible reaction.[38] Therefore AuNPs/PEDOT/CNTs/GCE has quasi-reversible property.

$$\Delta E = E_{pa} - E_{pc} \quad (1)$$

$$|I_{pa}/I_{pc}| = 1 \quad (2)$$

The diffusion coefficient values for each modified electrode were calculated according to the Randles–Sevcik eqn (3) (Table 1). The results showed that, compared with other modified electrodes, the AuNPs/PEDOT/CNTs modified electrode has the highest diffusion rate of 8.0×10^{-6} cm^2 s^{-1}. The thickness of the diffusion layer increases with time, and the $[Fe(CN)_6]^{4-}$ ions in solution diffuse on the surface of the modified electrode because there is no agitation during the analysis, which results in a short diffusion layer and greater electron transfer rate. It can be seen from the Nyquist plots (Fig. 4(b)) that the modified electrode has a smaller charge transfer resistance R_{ct}, which is about 70.59 ohms. The Nyquist plots consists of two parts, the semicircular in the higher frequency region involves in the electron transfer limited process, and the linear part at lower frequency region stands for diffusion-limited process of the electrochemical reaction in this experiment. Scan rate of

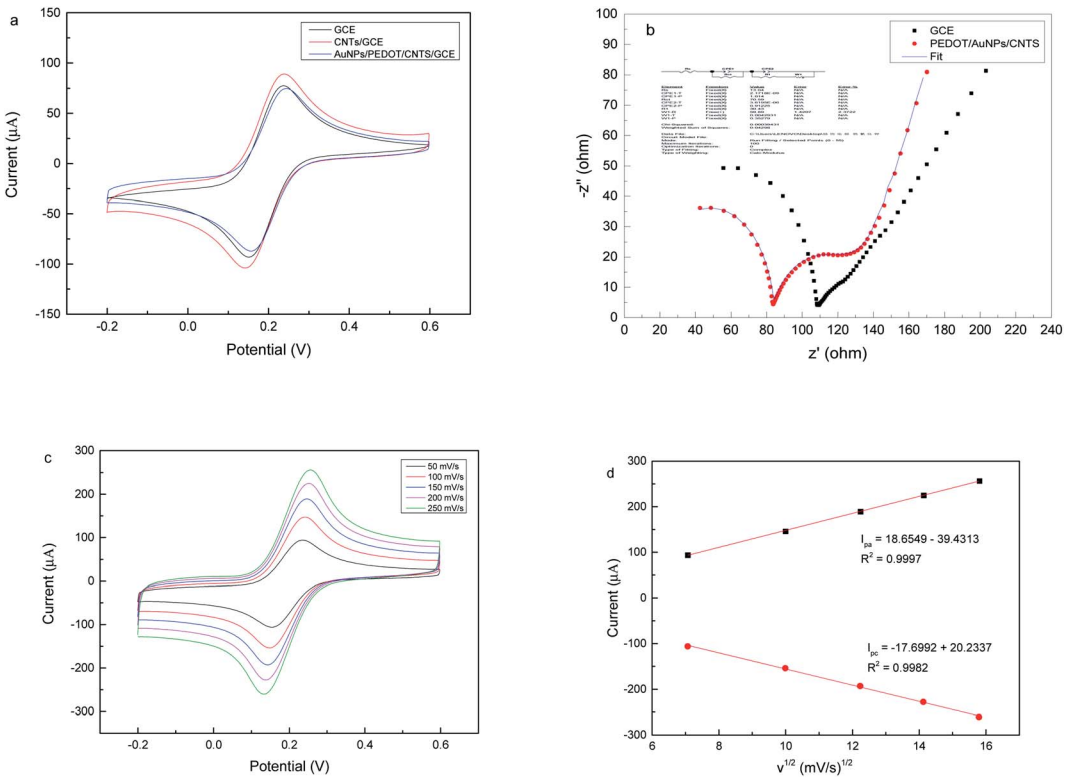

Fig. 4 (a) Cyclic voltammograms of different modified electrodes in 5 mM $K_4[Fe(CN)_6]$ and 0.1 M KCl mixture, (b) electrochemical impedance diagrams of different modified electrodes, (c) cyclic voltammograms of different scan rates of AuNPs/PEDOT/CNTs/GCE in a mixture of 5 mM $K_4[Fe(CN)_6]$ and 0.1 M KCl, (d) the relationship between the square root of scan rate and current density.

Table 1 Bare GCE, CNTs/GCE, AuNPs/PEDO and AuNPs/PEDOT/CNTs relationship between the square root of scan rate and peak current

Modified electrode	v (mV s^{-1})	$v^{1/2}$	Peak current (μA) I_{pa}	Peak current (μA) I_{pc}	R^2 (I_{pa} *vs.* $v^{1/2}$)	R^2 (I_{pc} *vs.* $v^{1/2}$)	Slope (I_{pa})	Slope (I_{pc})	E_{pa} (mV)	E_{pc} (mV)	ΔE (mV)	10^{-6} D (cm^2 s^{-1})
Bare GCE	50	7.07	75.59	−87.73	0.9988	0.9987	11.100	−10.379	249	164	85	8.0
	100	10.00	105.60	−121.1					255	158	97	
	150	12.25	133.50	−142.4					258	154	104	
	200	14.14	153.20	−162.4					261	151	110	
	250	15.81	171.90	−179					264	149	115	
CNTs/GCE	50	7.07	74.6	−87.71	0.9959	0.9964	12.5469	−12.6250	245	158	87	7.9
	100	10.00	113.8	−122.5					251	152	99	
	150	12.25	143.1	−149.8					254	147	107	
	200	14.14	167.4	−173.1					259	143	116	
	250	15.81	182.7	−199.6					263	139	124	
AuNPs/PEDOT/CNTs	50	7.07	93.46	−107.1	0.9997	0.9982	18.6549	−17.6992	237	155	82	9.9
	100	10.00	145.7	−155.1					243	149	94	
	150	12.25	188.9	−194.3					248	144	104	
	200	14.14	224.5	−229.2					253	139	114	
	250	15.81	256	−262.2					257	135	122	

100 mV s^{-1} was chosen because fast analysis was required and ΔE was closer to the theoretical value.

$$I_p = 0.4463nFAc(nFvD/RT)^{1/2} \quad (3)$$

3.3 Redox behavior of dopamine

The electro-oxidation of DA was analyzed by CV to explore the electrochemical behavior of the modified electrode in neutral buffer solution and DA mixed solution. The results showed that the AuNPs/PEDOT/CNTs/GCE has the highest oxidation peak current for dopamine detection, which indicates that the modified electrode has the best detection ability. This may be related to the synergistic effect between gold nanoparticles, acidified carbon nanotubes and PEDOT. By studying the effect of different scan rates on the dopamine response, it was found that the redox peak current was proportional to the scan rate, and the characteristic peak potential did not change much, which indicated that the electron-transfer reaction of dopamine at the electrode surface is a diffusion-controlled process,[38] the reaction kinetics between the redox sites is stable (Fig. 5).

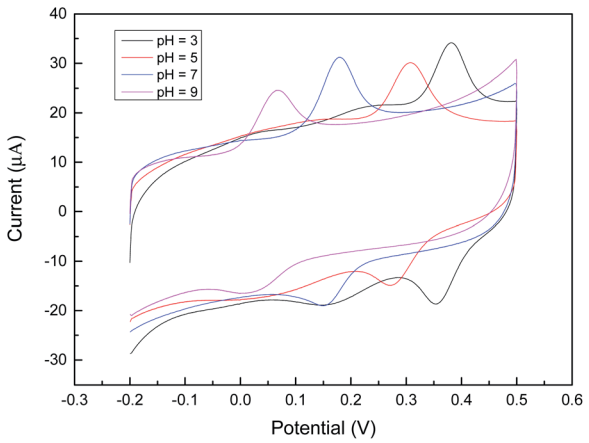

Fig. 6 Cyclic voltammograms of AuNPs/PEDOT/CNTs modified electrodes in PBS buffer solution (0.1 M) containing 9.14 μM DA at different pH values.

The effect of pH on AuNPs/PEDOT/CNTs modified electrodes was investigated by CV in 0.1 M PBS solutions with pH values of 3, 5, 7, 9, and 12 (Fig. 6). It can be seen that a higher redox peak

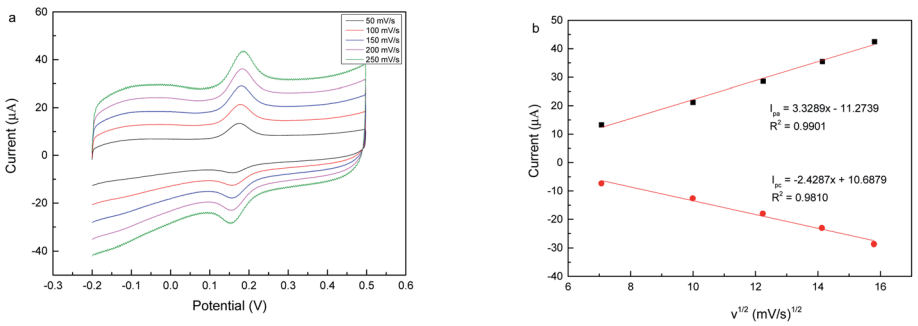

Fig. 5 (a) Cyclic voltammograms of AuNPs/PEDOT/CNTs modified electrodes at different scan rates in PBS buffer solution (0.1 M) containing 9.14 μM DA, (b) relationship between the square root of scan rate and peak current.

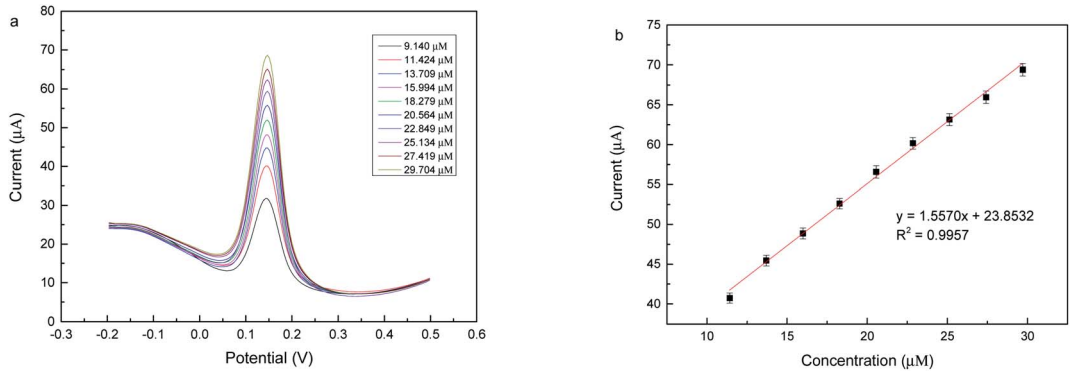

Fig. 7 (a) DPV of AuNPs/PEDOT/CNTs modified electrode with different DA concentrations in (pH = 7) 0.1 M PBS solution, (b) relationship between peak current and DA concentration.

is displayed under neutral conditions, and a lower redox peak is displayed under acid–base conditions, which indicates that DA can be effectively oxidized under neutral conditions and acidic conditions. Under alkaline conditions, the positively charged DA is not easily accessible to the surface of the modified electrode; under alkaline conditions, the stability of DA decreases,[39,40] resulting in the ineffective oxidation of DA. The peak potential shifted negatively with increasing pH, which confirmed that protons were involved in the oxidation of DA. In order to sensitively detect dopamine in the AuNPs/PEDOT/CNTs/GCE, a buffer solution of pH = 7 was selected, and the conditions were also closer to human serum.

In order to study the electrocatalytic performance of the AuNPs/PEDOT/CNTs modified electrodes, we further investigated the linear concentration range, sensitivity and detection limit of the modified electrodes for DA detection by DPV. The DPV curve changes were shown in Fig. 7. It can be seen from Fig. 7(b) that the oxidation peak current of DA in 0.1 M PBS (pH = 7) increases linearly with the concentration of DA in the range of 9.14–29.704 μM, the sensitivity is 1.557 μA μM^{-1}, and the detection limit LOD is 0.283 μM. Compared with other literature, it shows better detection performance (Table 1).

In order to evaluate the detection performance of the modified electrode under the interference of high concentrations of ascorbic acid AA and uric acid UA, we tested its anti-interference ability by continuously adding DA to the buffer solution mixed with 0.35 mM AA and 0.013 mM UA. It can be seen from Fig. 8 that the modified electrode can still detect DA well at high concentrations of AA and UA. For the bare electrode, since the characteristic peak potentials of DA, AA and UA are similar, they are often indistinguishable during detection. The modified electrode can distinguish the three substances, which may be related to the carboxyl functional group on the surface of the modified material. Since DA is positively charged, it can be specifically adsorbed on the surface of the modified material while repelling negatively charged AA. Under the condition of high concentration of interfering substances, the modified electrode still showed a good linear detection range, the detection limit LOD was 0.75 μM, and the sensitivity was 1.1051 μA μM^{-1} (Table 2).

Table 2 Electrochemical detection of dopamine with different modified electrodes

Sensing material	Linear range	LOD	Reference
Pd/rGO	6–469.5 μM	2.3 μM	41
PEDOT/AuNPs	0.15–330 μM	0.07 μM	36
Au/rGO/GCE	6.8–41 μM	1.4 μM	42
Au–Pd alloy nanoparticles	1.2–160 μM	0.83 μM	43
CNS/Pt/PANI/GCE	10–80 μM	0.6 μM	44
Poly(phenosafranine)	50–500 μM	20 μM	45
AuNPs/PEDOT/CNTs	9.14–29.704 μM	0.286 μM	This work

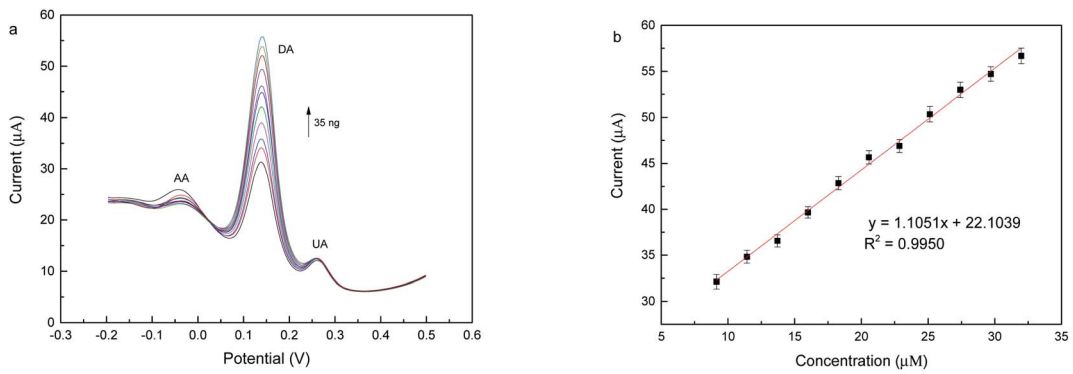

Fig. 8 (a) DPV at different DA concentrations in 0.1 M PBS containing 0.35 mM AA and 0.013 mM UA, (b) peak current *versus* concentration.

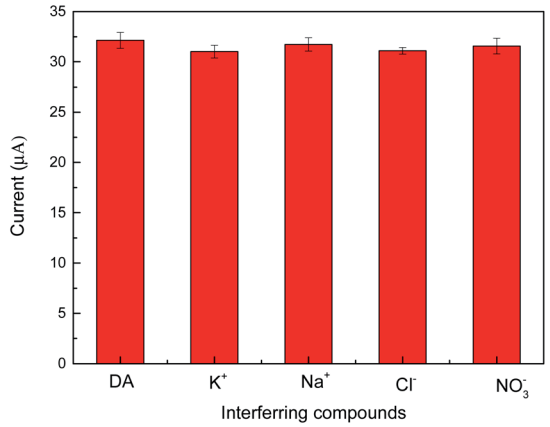

Fig. 9 Interference behavior of other ions in the detection of DA.

Table 3 Determination of DA content in dopamine hydrochloride

Sample (DA injection)	Theoretical value (μM)	Detection value (μM)	Recovery rate%
Sample 1	5.273	5.001	95.00
Sample 2	10.549	10.474	99.32
Sample 3	15.819	16.589	104.86
Sample 4	21.093	22.943	108.77
Sample 5	26.366	29.571	112.16

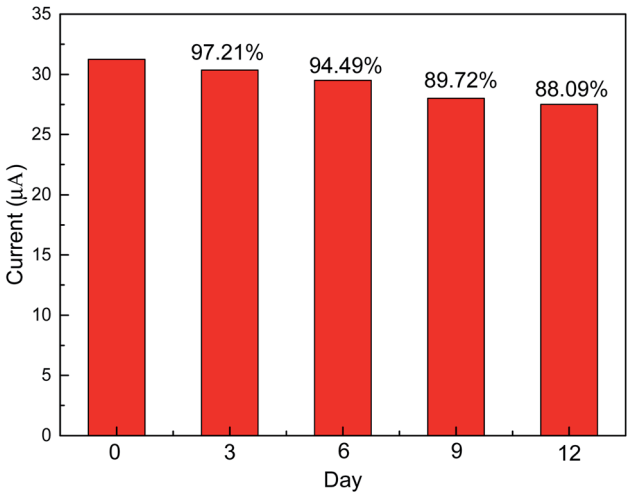

Fig. 10 Stability of modified electrode.

We also tested the response of the modified electrode to DA in the presence of other interfering compounds ions, such as K^+, Na^+, Cl^- and NO_3^-. The concentration of each interfering compounds ion is 1 mM. According to the change of current in Fig. 9, these ions hardly interfere with DA.

3.4 Detection in real sample

The detection accuracy of the modified electrodes was investigated by injecting dopamine hydrochloride. Dopamine hydrochloride for injection was accurately added to the PBS blank solution after dilution, and the detection results of the modified electrode are shown in Table 3. It can be seen that the modified electrode has high accuracy and precision.

The stability of AuNPs/PEDOT/CNTs modified electrodes stored at room temperature was investigated by DPV. The modified electrode was tested for its response to 9.14 μM DA in PBS buffer solution every 3 day, and the corresponding reaction results are shown in Fig. 10. It can be seen that the response of the modified electrode decreased by 2.79%, 5.51%, 10.28% and 11.91%, respectively. This indicates that the modified electrode has excellent stability.

4 Conclusions

In conclusion, the modified electrodes prepared by a facile one-pot method using AuNPs/PEDOT/CNTs as composite materials exhibited good performance. It has a limit of detection LOD of 0.283 μM and a sensitivity of 1.557 μA μM^{-1}. Under the interference of high concentrations of AA and UA, it showed excellent anti-interference ability. During the actual detection of samples, excellent accuracy is shown. High reproducibility and stability are maintained after a period of storage at room temperature. Nonetheless, its detection capability needs to be further improved. The composites based on AuNPs/PEDOT/CNTs are expected to be promising candidates for the detection of electroactive species.

Conflicts of interest

There are no conflicts to declare.

Acknowledgements

This work was supported by the University Natural Science Research Project of Anhui (KJ2020A0475, KJ2020A0472), National Innovation Training Program for College Students (202110878004) and Major Special Projects of Science and Technology of Anhui Province (201903a07020002).

References

1 Y. Wang, L. Wang and Q. Zhuang, *J. Alloys Compd.*, 2019, **802**, 326–334.
2 S. Reddy, Q. Xiao, H. Liu, C. Li, S. Chen, C. Wang, K. Chiu, N. Chen, Y. Tu, S. Ramakrishna and L. He, *ACS Appl. Mater. Interfaces*, 2019, **11**, 18254–18267.
3 I. M. Taylor, E. M. Robbins, K. A. Catt, P. A. Cody, C. L. Happe and X. T. Cui, *Biosens. Bioelectron.*, 2017, **89**, 400–410.
4 P. R. Da Silva Ribeiro and R. M. Duarte, *Braz. J. Pharm. Sci.*, 2014, **50**, 573–582.
5 I. Da Cruz Vieira and O. Fatibello-Filho, *Talanta*, 1998, **46**, 559–564.
6 X. Wei, Z. Zhang and Z. Wang, *Microchem. J.*, 2019, **145**, 55–58.
7 J. Peng, C. L. Han, J. Ling, C. J. Liu, Z. T. Ding and Q. E. Cao, *Luminescence*, 2018, **33**, 168–173.

8 L. Dong, Y. Zhang, X. Duan, X. Zhu, H. Sun and J. Xu, *Anal. Chem.*, 2017, **89**, 9695–9702.
9 B. Vellaichamy, P. Periakaruppan and T. Paulmony, *J. Phys. Chem. B*, 2017, **121**, 1118–1127.
10 S. S. Shankar, B. E. K. Swamy and B. N. Chandrashekar, *J. Mol. Liq.*, 2012, **168**, 80–86.
11 K. K. Kumar, M. Devendiran, R. A. Kalaivani and S. S. Narayanan, *New J. Chem.*, 2019, **43**, 19003–19013.
12 D. Li, K. Ao, Q. Wang, P. Lv and Q. Wei, *Molecules*, 2016, **21**, 618.
13 S. Han, T. Du, L. Lai, X. Jiang, C. Cheng, H. Jiang and X. Wang, *RSC Adv.*, 2016, **6**, 82033–82039.
14 Q. Cao, P. Puthongkham and B. J. Venton, *Anal. Methods*, 2019, **11**, 247–261.
15 D. Sun, H. Li, M. Li, C. Li, H. Dai, D. Sun and B. Yang, *Sens. Actuators, B*, 2018, **259**, 433–442.
16 L. Wang, T. Meng, D. Zhao, H. Jia, S. An, X. Yang, H. Wang and Y. Zhang, *Biosens. Bioelectron.*, 2020, **148**, 111834.
17 L. Wang, T. Meng, G. Yu, S. Wu, J. Sun, H. Jia, H. Wang, X. Yang and Y. Zhang, *Biosens. Bioelectron.*, 2019, **124–125**, 53–58.
18 T. Meng, H. Jia, S. An, H. Wang, X. Yang and Y. Zhang, *Sens. Actuators, B*, 2020, **323**, 128621.
19 L. Wang, T. Meng, L. Liang, J. Sun, S. Wu, H. Wang, X. Yang and Y. Zhang, *Sens. Actuators, B*, 2019, **278**, 133–139.
20 D. Wen, W. Liu, A. K. Herrmann, D. Haubold, M. Holzschuh, F. Simon and A. Eychmüller, *Small*, 2016, **12**, 2439–2442.
21 X. Mei, Q. Wei, H. Long, Z. Yu, Z. Deng, L. Meng, J. Wang, J. Luo, C. Te Lin, L. Ma, K. Zheng and N. Hu, *Electrochim. Acta*, 2018, **271**, 84–91.
22 Q. Cao, P. Puthongkham and B. J. Venton, *Anal. Methods*, 2019, **11**, 247–261.
23 P. Puthongkham, C. Yang and B. J. Venton, *Electroanalysis*, 2018, **30**, 1073–1081.
24 Y. Yang, M. Li and Z. Zhu, *Talanta*, 2019, **201**, 295–300.
25 C. Yang, E. Trikantzopoulos, C. B. Jacobs and B. J. Venton, *Anal. Chim. Acta*, 2017, **965**, 1–8.
26 B. Vellaichamy, P. Periakaruppan and T. Paulmony, *J. Phys. Chem. B*, 2017, **121**, 1118–1127.
27 Y. Zhang, D. Deng, X. Zhu, S. Liu, Y. Zhu, L. Han and L. Luo, *Anal. Chim. Acta*, 2018, **1042**, 20–28.
28 B. Yang, J. Wang, D. Bin, M. Zhu, P. Yang and Y. Du, *J. Mater. Chem. B*, 2015, **3**, 7440–7448.
29 J. Zou, J. F. Guan, G. Q. Zhao, X. Y. Jiang, Y. P. Liu, J. G. Yu and W. J. Li, *J. Environ. Chem. Eng.*, 2021, **9**, 105831.
30 B. Hu, Y. Liu, Z. W. Wang, Y. Song, M. Wang, Z. Zhang and C. Sen Liu, *Appl. Surf. Sci.*, 2018, **441**, 694–707.
31 X. Wan, S. Yang, Z. Cai, Q. He, Y. Ye, Y. Xia, G. Li and J. Liu, *Nanomaterials*, 2019, **9**, 1–16.
32 K. K. Kumar, M. Devendiran, R. A. Kalaivani and S. S. Narayanan, *New J. Chem.*, 2019, **43**, 19003–19013.
33 D. Li, K. Ao, Q. Wang, P. Lv and Q. Wei, *Molecules*, 2016, **21**, 618.
34 M. A. Kafi, A. Paul, A. Vilouras and R. Dahiya, *Biosens. Bioelectron.*, 2020, **147**, 111781.
35 X. Luo, C. L. Weaver, D. D. Zhou, R. Greenberg and X. T. Cui, *Biomaterials*, 2011, **32**, 5551–5557.
36 A. Ali, R. Jamal, T. Abdiryim and X. Huang, *J. Electroanal. Chem.*, 2017, **787**, 110–117.
37 M. M. Oliveira and A. J. G. Zarbin, *J. Phys. Chem. C*, 2008, **112**, 18783–18786.
38 F. Yusoff, A. R. Rosli and H. Ghadimi, *J. Electrochem. Soc.*, 2021, **168**, 026509.
39 T. V. Sathisha, B. E. Kumara Swamy, M. Schell and B. Eswarappa, *J. Electroanal. Chem.*, 2014, **720–721**, 1–8.
40 M. Cheng, X. Zhang, M. Wang, H. Huang and J. Ma, *J. Electroanal. Chem.*, 2017, **786**, 1–7.
41 J. Wang, B. Yang, J. Zhong, B. Yan, K. Zhang, C. Zhai, Y. Shiraishi, Y. Du and P. Yang, *J. Colloid Interface Sci.*, 2017, **497**, 172–180.
42 C. Wang, J. Du, H. Wang, C. Zou, F. Jiang, P. Yang and Y. Du, *Sens. Actuators, B*, 2014, **204**, 302–309.
43 C. Zhou, S. Li, W. Zhu, H. Pang and H. Ma, *Electrochim. Acta*, 2013, **113**, 454–463.
44 G. Alarcón-Angeles, B. Pérez-López, M. Palomar-Pardave, M. T. Ramírez-Silva, S. Alegret and A. Merkoçi, *Carbon*, 2008, **46**, 898–906.
45 K. Miyazaki, G. Matsumoto, M. Yamada, S. Yasui and H. Kaneko, *Electrochim. Acta*, 1999, **44**, 3809–3820.